Hindawi
Journal of Nanomaterials
Volume 2019, Article ID 6105818, 13 pages
https://doi.org/10.1155/2019/6105818

Research Article

Biocompatibility of Developing 3D-Printed Tubular Scaffold Coated with Nanofibers for Bone Applications

Febe Carolina Vazquez-Vazquez,[1] Osmar Alejandro Chanes-Cuevas,[1] David Masuoka,[2] Jesús Arenas Alatorre,[3] Daniel Chavarria-Bolaños,[4] José Roberto Vega-Baudrit,[5] Janeth Serrano-Bello,[1] and Marco Antonio Alvarez-Perez[1]

[1]*Laboratorio de Bioingeniería de Tejidos, División de Estudios de Posgrado e Investigación de la Facultad de Odontología, UNAM, Circuito Exterior, s/n., Cd. Universitaria, 04510 Coyoacán, CDMX, Mexico*
[2]*Facultad de Estomatología, Universidad Autónoma de Aguascalientes, Aguascalientes, Mexico*
[3]*Instituto de Física, UNAM, Circuito Exterior, s/n., Cd. Universitaria, 04510 Coyoacán, CDMX, Mexico*
[4]*Facultad de Odontología, Universidad de Costa Rica, Costa Rica*
[5]*LANOTEC, San José, Costa Rica*

Correspondence should be addressed to Marco Antonio Alvarez-Perez; marcoalv@unam.mx

Received 19 February 2019; Accepted 28 March 2019; Published 9 May 2019

Guest Editor: Min-Suk Kook

3D printing with controlled microarchitectures has gained traction in a wide variety of fields, including bone tissue engineering, because it represents an exciting alternative for the synthesis of new scaffolds due to its rapid manufacturing process, high precision, cost-effectiveness, and ease of use. Thus, this study is aimed at evaluating the biocompatibility response of a 3D-printed tubular scaffold coated by a layer of 7% PLA nanofibers. The morphology, structure, and chemical composition of the 3D-printed tubular scaffold were characterized by scanning electron microscopy (SEM), X-ray diffraction (XRD), Fourier Transform Infrared (FTIR), thermogravimetric analysis (TGA), differential scanning calorimetry (DSC), and surface property analysis by profilometry. The biocompatibility response of the scaffold was assessed by cell adhesion, proliferation, and cell-material interactions of human fetal osteoblasts. Our results showed that 3D printing allowed obtaining similar and reproducible structures and the biocompatibility assays showed that nanofiber coating of the surface of the 3D tubular scaffold promoted an improvement on cell attachment, proliferation, and the morphology of osteoblast cells when compared with a noncoated scaffold. In conclusion, the surface of the 3D-printed tubular scaffold could be improved by the deposition of a nanofiber layer to render a more mimetic and active topography with excellent cellular biocompatibility for bone tissue applications.

1. Introduction

Bone defects have a high impact on a patient's quality of life, leading to a high demand for bone substitutes in the orthopedic and maxillofacial fields. Moreover, current surgical procedures for bone regeneration utilize transplantation (auto- and allografts) that must deal with the repair, renewal, and replacement of the bone tissue defect. However, these treatments have severe drawbacks such as donor site morbidity, severe pain, unavailability of large tissue volumes, risk of infections, immunogenicity, and the risk of communicable diseases [1–4].

Bone tissue engineering has emerged as promising strategies to replace or regenerate critical bone size defects with the ambition of circumventing the complications associated with traditional techniques [5–7]. Current procedures involve the construction of a scaffold with a combination of materials and cells [8]. The ideal scaffold should be tailored to mimic the native tissue characteristics to facilitate localization and distribution of a cell to specific sites in the body,

maintain a three-dimensional architecture (3D), have a highly porous structure with an interconnected network for cell growth and flow transport of nutrients and metabolic waste, and be biocompatible and nontoxic, with optimal physical and mechanical properties that allow and guide the formation of new tissues with an appropriate function [9]. However, one of the biggest challenges for bone tissue engineering is to design a 3D scaffold structure that could mimic the *in vivo* extracellular matrix and cell environment because cells lack the ability to grow in favored 3D orientations by themselves. Moreover, one of the critical factors to bridge this gap is the possibility of modulating scaffold characteristics so that specific biological, clinical, manufacturing, economic, and regulatory prerequisites can be met [10].

In recent years, 3D printing or additive manufacturing techniques have emerged as a useful tool for the generation of 3D scaffolds with controlled microarchitectures and have gained traction in bone tissue engineering because they represent an attractive alternative technique for the synthesis of new scaffolds allowing the modulation and control of the geometry with high precision over the pore size, porosity, and outer shape of the scaffold. They could also be used to reproduce specific bone defect shapes because of their rapid manufacturing process, cost-effectiveness, and ease of use [11–13]. Thus, 3D printing in the synthesis of bone scaffolds has been used due to its high flexibility in biocompatible, biodegradable, and biocomposite polymeric material handling [13–18]. In particular, in the 3D printing technique, polylactic acid (PLA) has been utilized to develop synthetic scaffolds. PLA is a linear aliphatic polyester which is widely used in bone tissue engineering because its mechanical integrity is preserved *in vitro* or *in vivo*, it is approved by the FDA, and it has extensively been used as a biomaterial in the human body for its adsorbability and nontoxicity after degradation, its thermoplastic properties, and its low viscosity [19]. 3D printing technology holds great promise for tissue engineering because 3D printing can easily control roughness at the micron scale; however, controlling roughness at the nanoscale level has proved more difficult. That is why it is necessary to improve the 3D-printed surface so that they promote cell interactions as well as mimic the nanotopography of natural bone. One strategy is to coat the 3D structure with a nanofiber layer to achieve a suitable surface for cell attachment, proliferation, and differentiation and provide an open, porous network for uniform cell distribution during cell seeding [20]. In this work, we propose the use of the air jet spinning technique (AJS) as a simple method for surface modification based on a specialized spinning system nozzle (such as a commercial airbrush), a surface for collecting polymer fibers, and compressed gas; through this method, the polymer solution and pressurized gas are simultaneously ejected to form the fiber morphology [21]. Thus, this work is aimed at synthesizing and fabricating 3D tubular scaffolds by using 3D printing to coat the surface of a printed scaffold with a layer of PLA fibers by AJS. The improved 3D-printed tubular scaffold was characterized by SEM, XRD, FTIR, TGA, and DSC, and the influence of the submicrometric fiber surface coating in the biological response of human fetal osteoblast cells (hFOB) on cell adhesion, cell-material interaction, and proliferation assays was evaluated.

2. Materials and Methods

2.1. Manufacture of 3D Tubular Scaffold. Cylindrical scaffolds were proposed using a dual technique that employs both an inner core of PLA built by 3D additive manufacturing and an outer layer functionalization of PLA nanofibers. The inner core geometries of the scaffold were digitally designed with Cura 3D printing software 3.0, and 3D tube scaffolds were fabricated by additive manufacturing (MakerMex Printers, León, México) of polylactic acid (PLA). The outer functionalization of the tubular scaffold was done by a cover with fiber spun mats fabricated with the air jet spinning technique (AJS). Briefly, PLA pellets ($C_3H_6O_3$; MW 192,000 from NatureWorks) were dissolved in chloroform/acetone (volume ratio of 3 : 1) to obtain a 7% (w/v) polymer solution. Then, the polymeric solution was placed in commercially available ADIR model 699 airbrushes with a 0.3 mm nozzle diameter and with a gravitational feed of the solution to synthesize the fiber membrane scaffold. The airbrush was connected to a pressurized argon tank (CAS number 7740-37, concentration > 99%, PRAXAIR México, CDMX, México), and a pressure of 35 psi and a distance of 10 cm from the nozzle to the 3D tubular scaffold were constantly maintained for fiber deposition.

2.2. Characterization of 3D Tubular Scaffold. 3D-printed tubular scaffolds were characterized by SEM, XRD, FTIR, topographical analysis, DSC, and TGA. The morphology and structure of the 3D tubular scaffold were observed by field emission scanning electron microscopy (JEOL JSM-7600F FE-SEM). The samples were sputter coated with 5 nm of a thin gold layer (EMS 150R, Quorum, USA) to analyze outer and inner surfaces. Specific observations were done to analyze the interphase between nanofibers and the core material. Scaffold structures were determined by XRD employing a D8 FOCUS Bruker AXS diffractometer with Cu-Kα radiation in the 2θ range between 5° and 50°. The chemical structure of 3D tubular scaffolds was analyzed by FTIR employing the IRAffinity-1S (Shimadzu, Kyoto, Japan) within the 400-4,000 cm^{-1} range. The topographic images were taken with a contact profilometer (Bruker Dektak XT, USA). A 2 μm radius needle tip was used. The sweep axis was taken with an applied force of 4 mg, and the resolution was adjusted to 0.033 μm/point (corresponding to a needle tip speed of 10 μm/s covering a total area of 500 × 500 μm). The image was constructed by joining 500 scans with a separation of 1 μm. The roughness values were evaluated using the entire measured area to determine the average roughness (Ra) and the average maximum depressions (Rq). TGA and DSC evaluated thermal response. TGA (TGA Q500, TA instruments, Delaware, USA) was done with 4-6 mg of each sample, running a ramp from 25°C to 1000°C, with a heating rate of 20°C/min. Onset point (To), inflection points (Tp), and maximum mass loss point (Tmax) were calculated. DSC (DSC Q200, TA instruments, Delaware, USA) was performed with 2.5-3 mg of each sample, running a ramp

from 25°C to 250°C, with a heating rate of 10°C/min. Glass transition temperature (Tg) and melting point (Tm) were calculated. Tg was confirmed by calculating the tan δ with a dynamic mechanical analysis (DMA) of the samples. DMA analysis began at 20°C, and a ramp of 3°C/min with a strain level of 0.1% and an angular frequency of 6.28 rads/s was used.

2.3. Processing of 3D Tubular Scaffold for Cell Seeding. Before the biological assays, 3D tubular scaffolds were placed in 24-cell culture plates and sterilized by immersion in 70% ethanol (*v*/*v*) with an antibiotic solution (streptomycin 100 μg/mL and penicillin 100 U/mL) for 30 min. After sterilization, nanofiber scaffolds were rinsed with PBS, washed with distilled water three times, and air-dried.

2.4. Cell Culture. Biological assays to evaluate the cell biocompatibility response of 3D tubular scaffolds were performed using human fetal osteoblasts (hFOB, 1.19 ATCC) cultured in a 75 cm^2 cell culture flask in Dulbecco's Modified Eagle Medium (DMEM, Corning) supplemented with 10% Fetal Bovine Serum (FBS, Corning), antibiotic solution (streptomycin 100 μg/mL, penicillin 100 U/mL, and fungizone 0.3 μg/mL, Sigma-Aldrich, USA), and 2 mM L-glutamine (Sigma-Aldrich, USA). For all the experimental procedures, hFOB cells at 2-6 passages were used and incubated at 37°C in a 100% humidified atmosphere with 5% CO_2 and 95% air.

2.5. Cellular Adhesion Assay. hFBO cells were seeded at 1×10^4 cells/mL onto 3D tubular scaffolds with and without a fiber layer coating placed in 24-well culture plates and allowed to adhere in a standard cell culture for 4 and 24 h. After the prescribed time, the 3D tubular scaffolds were rinsed three times employing PBS to remove nonadherent cells. The evaluation of cell attachment was performed according to a crystal violet assay. Briefly, adherent cells were fixed with 4% paraformaldehyde and incubated with 0.1% crystal violet solution for 15 min. Then, the dye was extracted with 0.1% of sodium dodecyl sulfate (SDS), and optical absorption was quantified by spectrophotometry at 545 nm with a plate reader (ChroMate, Awareness Technology).

2.6. Cell Proliferation Assay. The cell viability of hFOB cells plated at a concentration of 1×10^4 cells/mL in triplicate onto 3D tubular scaffolds with and without a fiber layer coating was checked by the WST-1 assay for 1, 3, 7, 14, and 21 days of culture. This assay is based on the ability of the mitochondrial succinate-tetrazolium reductase of living cells to reduce a WST-1 salt (4-(3-(4-iodophenyl)-2-(4-nitrophenyl)-2H-5-tetrazolio)-1,3-benzene disulfonate) to produce a water-soluble formazan dye product. The concentration of the formazan product is directly proportional to the number of metabolically active cells. hFOB cells seeded onto a 3D tubular scaffold at the prescribed times were washed with PBS and incubated with 400 μL fresh culture medium containing 40 μL of the cell proliferation reagent WST-1 for 4 h at 37°C. Then, 200 μL of the supernatant was removed, and the absorbance was quantified by spectrophotometry at 450 nm with a plate reader (ChroMate, Awareness Technology). During the experimental time, the culture medium was exchanged every other day with fresh media.

2.7. Cell Morphology. The cell morphology, spreading pattern, and cell-material interaction of hFOB cells seeded at 1×10^4 cells/mL onto 3D tubular scaffolds with and without a fiber layer coating were examined using SEM and fluorescence microscopy (AMSCOPE) after 24 h of cell culture. For SEM analysis, at the end of the incubation culture time, 3D tubular scaffolds were washed three times with PBS, fixed with 2% glutaraldehyde for 1 h, and then dehydrated with a graded series of ethanol (25-100%); finally, samples were subjected to critical point drying. The samples were sputter coated with a thin layer of gold-palladium and examined by SEM.

For fluorescence microscopy, before seeding onto 3D tubular scaffolds, the hFOB culture cells were incubated with CellTracker™ Green CMFDA (5-chloromethylfluorescein diacetate) in phenol red-free medium at 37°C for 30 min. Subsequently, the cell culture was washed with PBS and incubated for 1 h in complete medium. After recovery, hFOB cells were trypsinized and counted to the desired cell concentration (1×10^4 cells/mL) and incubated for 24 h onto 3D tubular scaffolds and evaluated for spreading and cell-material interaction.

2.8. Statistical Analysis. All quantitative data were expressed as the average ± standard error of the mean. Numerical data were analyzed via Student's *t*-test to determine the differences among the groups. Statistical significance was considered at $p < 0.05$.

3. Results and Discussion

3.1. Morphological Characterization of 3D Tubular Scaffold. This study is aimed at creating a polymeric scaffold by combining two different techniques: 3D printing and air jet spinning (AJS). The morphological, physicochemical, and biological properties of this innovative option were also evaluated. The approach to fabricate a bicomponent scaffold that could mimic the extracellular matrix and morphology of long bone structures was followed first by the creation of a cylindrical core built by additive printing of PLA to acquire the mechanical properties for long bones and then by adding a coating of PLA fibers obtained by air jet spinning to mimic Sharpey's fibers of compact bones in the periosteum. 3D-printed tubular scaffolds were observed using SEM both at high and low magnification micrographs. Both 3D tubular scaffolds (Figures 1(a), 1(b), 1(d), and 1(e)) and 3D tubular scaffolds coated with fibers (Figures 2(a), 2(b), 2(d), and 2(e)) analyzed at low magnification showed a similar macrostructure with similar geometry and homogeneous nonporous microtopography with evident wrinkles which exhibit small extruded triangle-shaped gaps. Moreover, 3D tubular scaffolds at high magnification micrographs (Figures 1(c) and 1(f)) showed a smooth homogeneous surface morphology of the polymer after the layer-by-layer deposition of the polymer, whereas the 3D tubular scaffolds coated with fibers

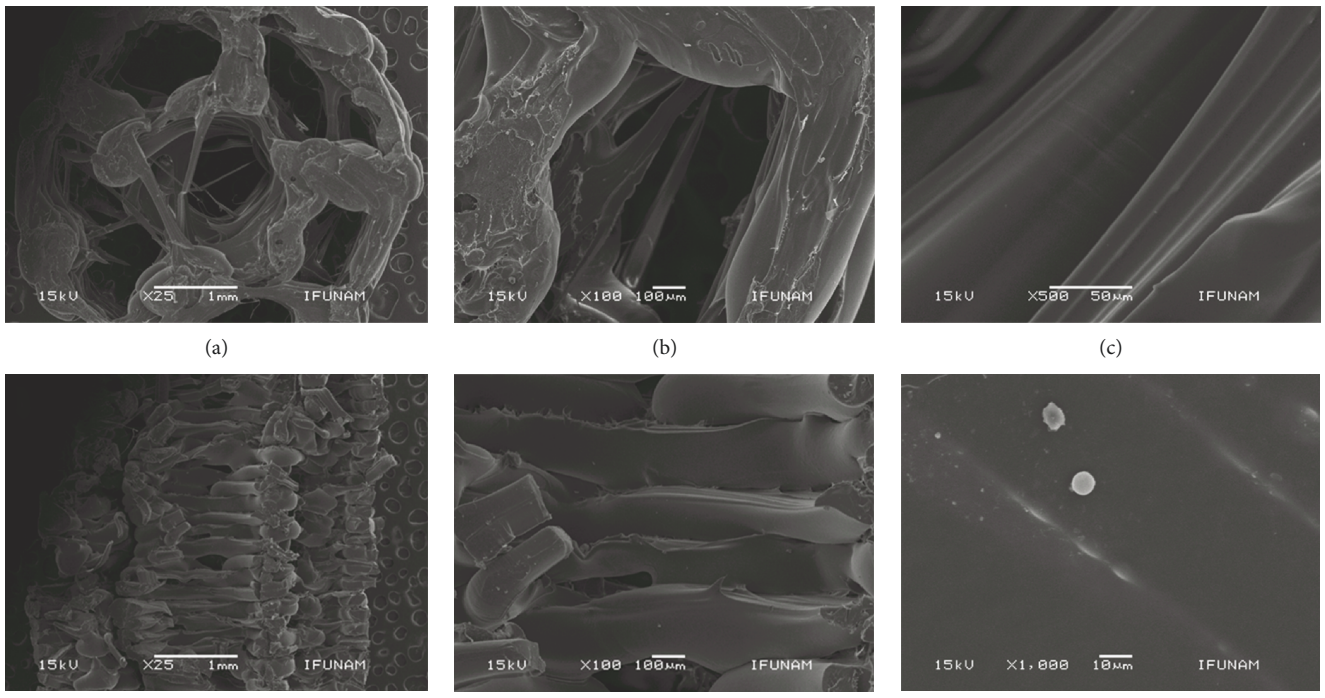

Figure 1: SEM micrographs showing the morphology of the 3D-printed tubular scaffold.

showed the interphase between the printed material and fiber layer, displaying a roughness morphology (Figures 2(c), 2(f), and 2(i)), which confirms the significant difference in the surface topography of the two scaffolds. Additionally, high magnification micrographs of the coating distribution showed the morphology of the random fibers with an average diameter of $0.430 \pm 0.205\,\mu$m demonstrating that the coating was well distributed in the printed matrix (Figures 2(g)–2(i)) that covers all of the surface giving a marked roughness in comparison with the scaffold alone. This finding further proved the suitability of the combination of the dual approach (3D printing and coating with AJS) to obtain a fiber layer dispersion well adapted to the 3D surface scaffold with a homogeneous thickness distribution of submicrometric fibers in all the areas, a thickness which could be dependent on the deposition time of coating. The deeper nanofibers showed good adaptation and merged with a printed scaffold. This is in agreement with studies that use additive manufacturing and rapid prototyping for producing composite constructs for tissue engineering applications [22–25].

3.2. Structural Characterization

3.2.1. XRD Analysis. The comparison of the crystalline structure of the PLA filament with that of the 3D tubular scaffold was further characterized by XRD (Figure 3). The diffractograms showed that both 3D tubular scaffolds have a signal with the same value as a broadband characteristic of an amorphous peak that increased significantly in comparison with the PLA filament with a lower intensity. These results are in concordance with different studies that reported that PLA is amorphous and depends on the crosslinking of dopants or printed parameters [26–29].

3.2.2. FTIR Analysis. The chemical identity for interpreting and determining the functional groups were analyzed using FTIR during the printing of the 3D tubular scaffolds. For a comparison of the 3D-printed scaffold spectra, the pure PLA filament and PLA fibers were also examined. The peak at $2922\,cm^{-1}$ is the stretching vibration absorption of C-H. Peaks were also observed at 758 and $873\,cm^{-1}$ (-CH bending vibration), 1043 and $1182\,cm^{-1}$ (C-O stretching vibration), $1450\,cm^{-1}$ ($-CH_3$ bending vibration), and $1751\,cm^{-1}$ (C=O stretching vibration on ester group) as shown the Figure 4. From the infrared spectra absorption, a slight difference could be seen between all samples. Moreover, these results are supported and in agreement with several studies that used FTIR to investigate the structural features of printing samples before and after extrusion and to analyze if the PLA filament does not contain any significant contaminants [23, 30–33].

3.2.3. Profilometry. The surface topographies of the 3D tubular scaffolds with and without coating with fibers were analyzed by profilometry (Figure 5). The results showed the smoothest topography of the 3D tubular scaffold with an average roughness (Ra) of $0.049\,\mu$m and average maximum depression (Rq) of $0.064\,\mu$m (Figure 5(a)), in comparison with the 3D tubular scaffold coated with fibers that showed the influence of the nanofibers on the average roughness (Ra) of $0.586\,\mu$m and the average maximum depression (Rq) of $0.727\,\mu$m (Figure 5(b)). These results are in concordance with SEM images and studies of 3D composite

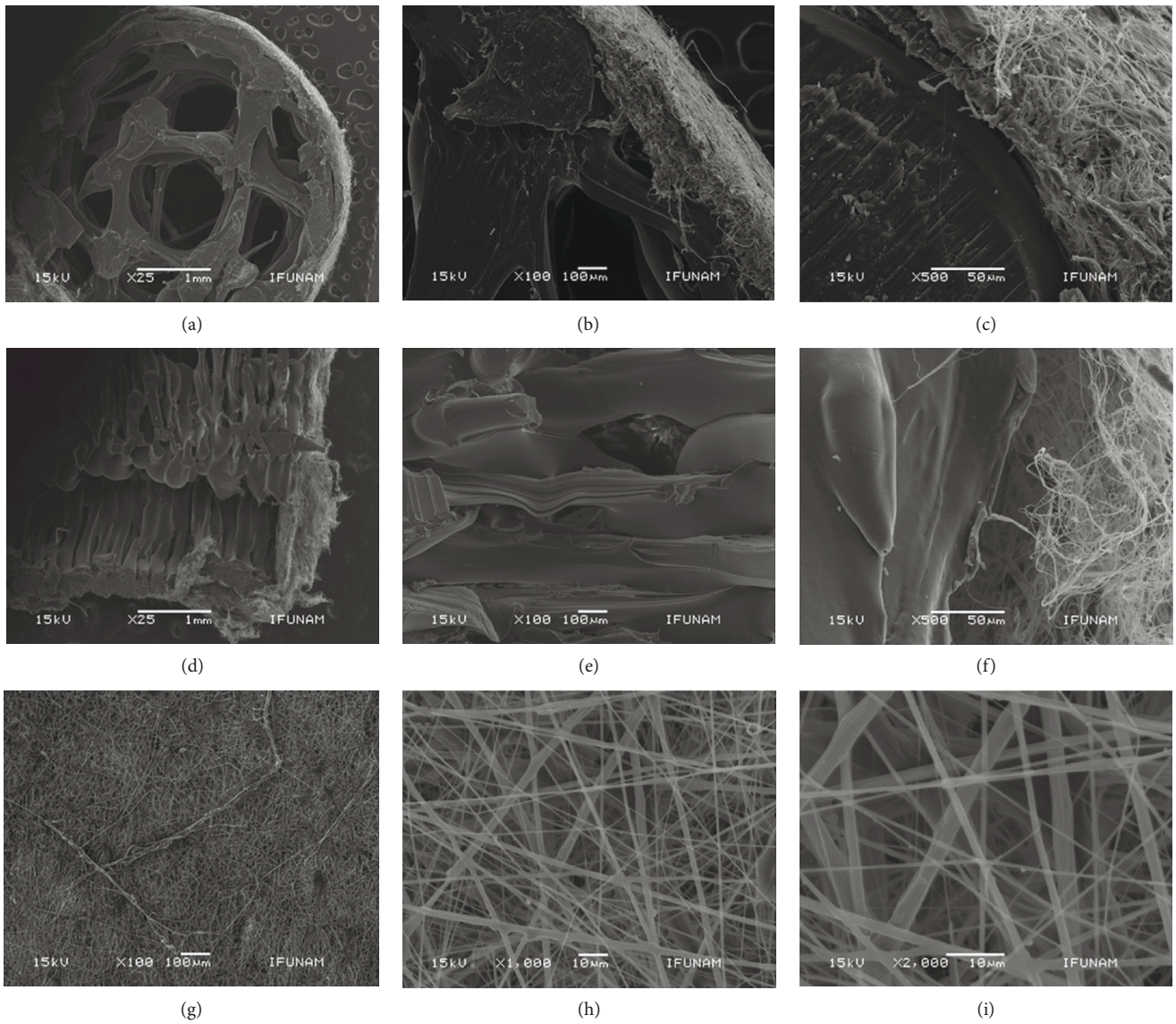

Figure 2: SEM micrographs of the 3D-printed tubular scaffold coated with 7% PLA nanofibers.

blends that reported the effect on the structural, surface, and morphological properties onto the scaffold with increased roughness values with clear peaks and valleys related to composites [25, 34–36]. Moreover, the coating of nanofibers is in agreement with a study where the adhesion properties of the 3D printing of polymers and nanocomposites onto textiles was analyzed; this study reported that the adhesion force of the deposited PLA and PLA nanocomposites onto the PLA fabrics was very strong, which was determined in all samples according to the strength of the deposited layer and structure [37].

3.3. Thermal Characterization. The thermal stability of the different 3D tubular scaffolds was analyzed by thermal gravimetric analysis (TGA) for measuring the weight change of the scaffolds as a function of the temperature in a controlled atmosphere. Derivative thermogravimetric analysis (DTG) was used to determine the decomposition temperature of the 3D scaffolds. From the spectra (Figure 6), the determination of the onset point (To), the inflection point (Tp), and the mass loss temperature (Tmax) of the 3D tubular scaffolds could be seen in comparison with the pure PLA filament as a single-stage degradation mechanism for all three samples. For the 3D tubular scaffold coated with fibers, the highest To = 331°C could be seen in comparison with the 3D tubular scaffold and pure PLA filament which both started their mass loss at 327°C. Moreover, the 3D tubular scaffold coated with fibers was completely degraded at around 369°C in comparison with the 3D tubular scaffold that degraded at 394°C and the pure PLA filament that degraded at 355°C. Finally, for DGT curve related to the inflection points, the 3D tubular scaffold showed an increase of the TGA curve of 21°C compared with the 3D tubular scaffold coated with fibers that led to an increase of 17°C; however, both 3D tubular scaffolds showed to be increased when compared with the pure PLA filament (Figure 6). Based on the TGA and DGT curves,

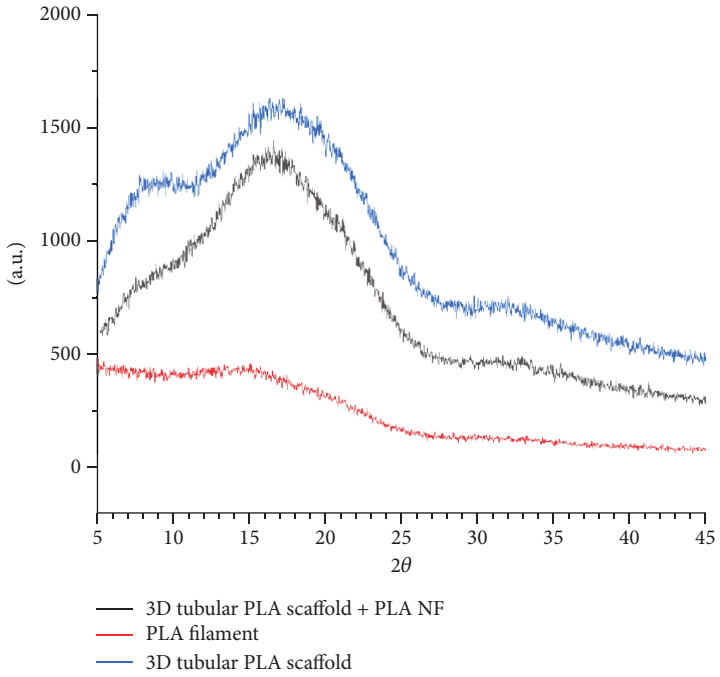

Figure 3: XRD patterns of the pure PLA filament (red), 3D tubular scaffold (blue), and 3D tubular scaffold coated with nanofibers (black).

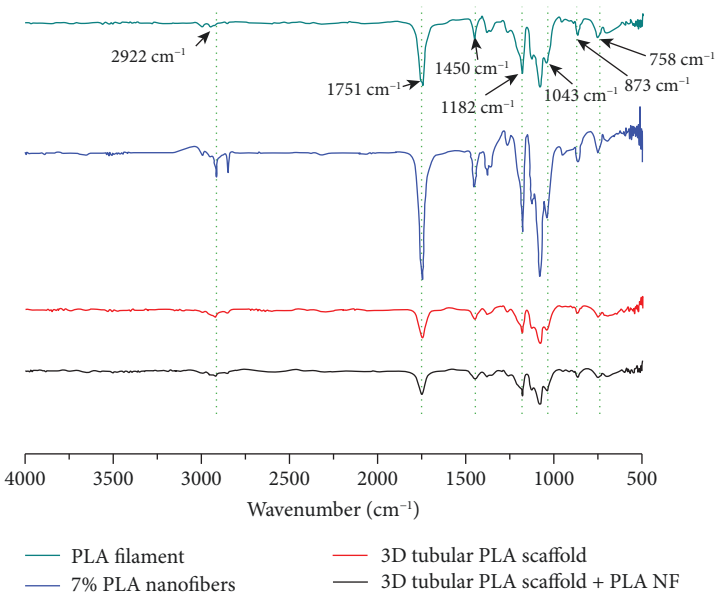

Figure 4: FTIR spectrum of the PLA filament (green), 7% PLA nanofibers (blue), 3D tubular scaffold (red), and 3D tubular scaffold coated with nanofibers (black) where group resonance was detected as peak signals identified with arrows.

the incorporation of the fiber layer coating by air jet spinning onto the tubular 3D-printed scaffold influenced the thermal degradation temperature which enhances the thermal stability of the scaffold. These results are in agreement with several studies that use TGA for analyzing the scaffold fabrication process considering that the polymer matrix is subjected to high temperatures. These results also show that (1) the polymer does not undergo changes in its properties and thus avoids any degradation phenomena due to the process, (2) the composites show an increase in the thermal stability properties of the scaffolds, and (3) the extrusion process does not have any influence on the chemical properties of the 3D sample scaffolds [30, 38–40].

Figure 7 shows the change of the thermal properties using the DSC curves for the set of studies of the following materials: pure PLA filament, 3D tubular scaffold, and 3D tubular scaffold coated with fibers. DSC analyses showed a similar behavior for the three samples, with a clear glass transition

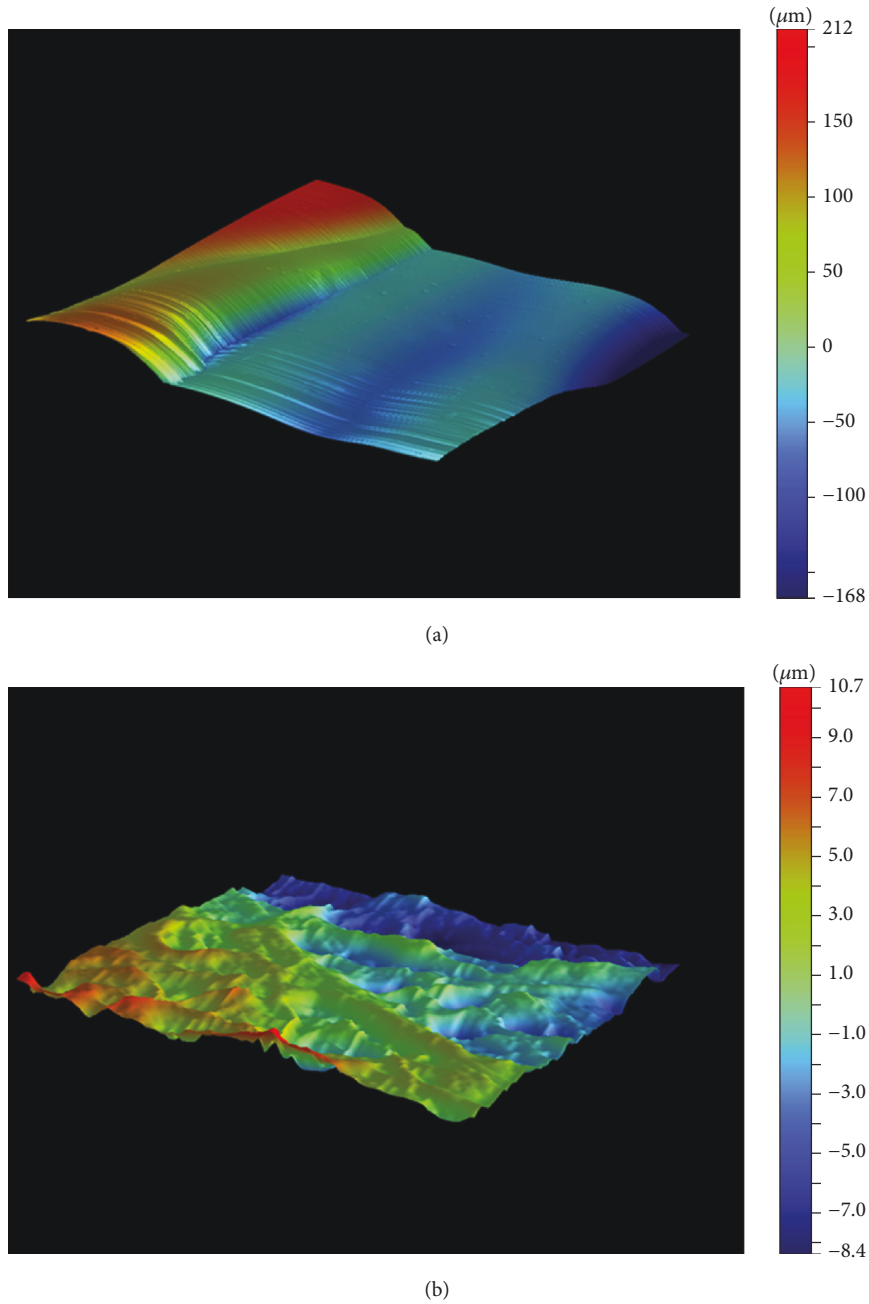

Figure 5: Optical profiler data showing the topography of a 3D-printed tubular scaffold. (a) Images show the uncoated smooth surface and (b) the coated surface where roughness is strongly enhanced by the presence of nanofibers.

point (Tg) between 56 and 62°C, followed by an exothermic signal and a marked melting point (Tm) around 169°C. When comparing the analyses of the three samples, pure PLA showed a lower Tg and a higher Tm, indicating that pure bulk PLA requires an increased heat flow to achieve a different physical state. It is possible that printed material with smaller polymeric structures, especially those functionalized with fibers, may easily distribute the heat flow achieving a faster melting point. DMA analyses supported these results (Figure 8), where the same behavior was observed. Pure PLA showed a tan (δ) of 70.4°C, while 3D tubular scaffolds (functionalized with and without fibers) showed an increased tan (δ) of 76°C. The thermal behavior of the analyzed materials is consistent with findings from the literature where it is reported that the processing parameters used to elaborate the scaffolds did not induce significant changes in terms of temperature and the variation is not substantial enough for affirming decomposition of the material. Moreover, the crystallization of PLA could be the result of the lamellar rearrangement of the polymer that depends on the molecular characteristics and composition, as well as the reorganization of less crystalline

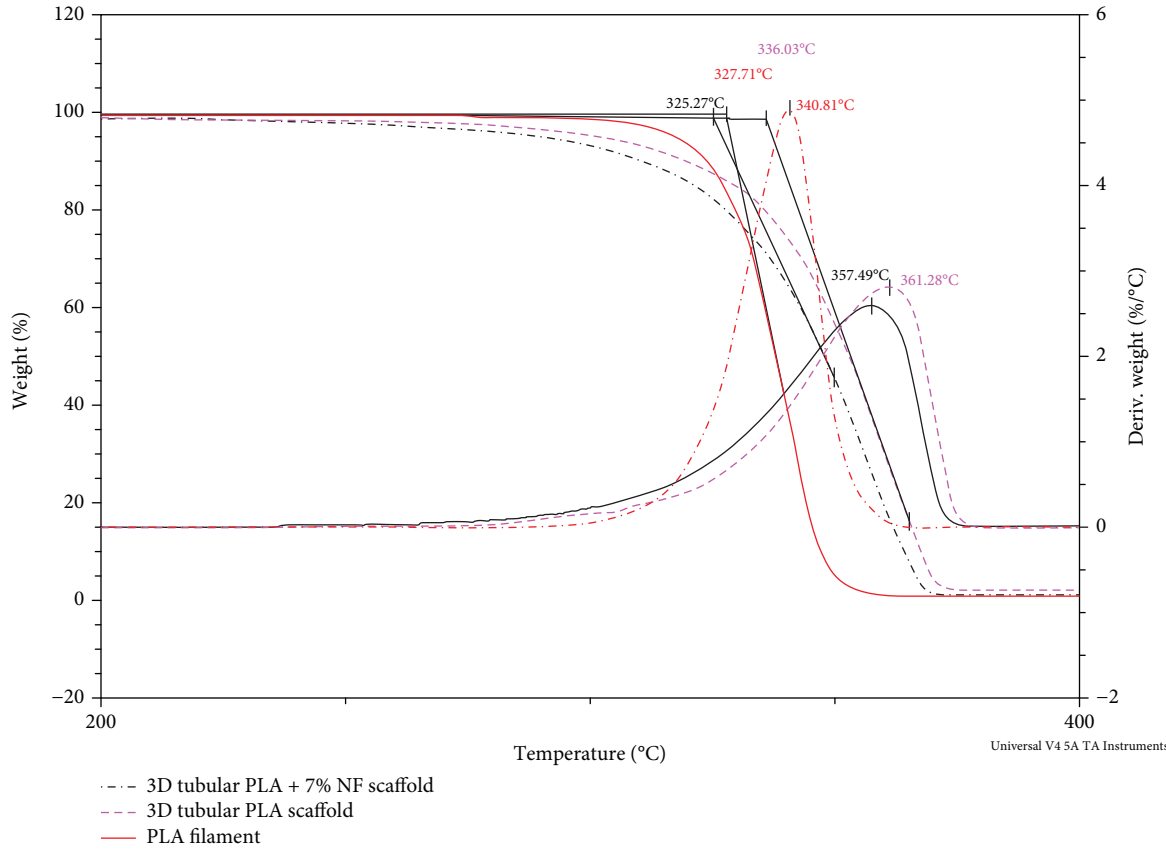

Figure 6: Thermogravimetric analysis (TGA) curves of the PLA filament and the 3D-printed tubular scaffolds with and without the nanofiber coating layer.

regions, resulting in the expansion of the amorphous areas [28, 35, 41–43]. This was also supported by the XRD analysis of the 3D tubular scaffolds.

3.4. Biological Evaluation of the 3D Tubular Scaffolds. The evaluation of the biocompatibility of osteoblast cells on the surface of biomaterials is a key step for bone tissue engineering and regeneration applications. For this reason, the response of cell adhesion of hFOB cells seeded onto 3D tubular scaffolds coated with and without fibers was analyzed by crystal violet according to the defined time intervals, as shown in Figure 9(a). As can be seen clearly, more cells adhered on the 3D tubular scaffold coated with nanofibers than on the 3D tubular scaffold; however, both 3D tubular scaffolds showed higher cell adhesion when compared with control PLA filament groups after 4 and 24 h of cell culture ($p < 0.05$). For the cell attachment study, the percent of cells in the 3D tubular scaffold coated with a fiber layer increased by 13% after 4 h and 15% after 24 h, when compared with the 3D tubular scaffold ($p < 0.05$). This indicates that the combination of the fiber membrane and rough surface morphologies played a decisive role in the attachment of human osteoblast cells supported by SEM and fluorescence analysis (Figures 10–12).

The cell viability of hFOB cells cultured onto 3D tubular scaffolds coated with and without fibers after seeding for 1, 3, 7, 14, and 21 days was characterized by the WST-1 assay (Figure 9(b)). The results showed that after 1 day of culture, the cell viability of hFOB cells cultured onto 3D tubular scaffolds is higher than that on the PLA filament, which is consistent with the results of cell attachment after 4 and 24 h of culture (Figure 9(a)). Moreover, the response of the cell that grew well over time and as incubation time increased could be seen; the cell viability increases onto the 3D tubular scaffolds during the experimental periods, and it could be seen that there was no significant difference in the cell response between scaffolds after culturing for 7-21 days ($p < 0.05$). These results showed that printed scaffolds did not induce any cytotoxicity effects on the behavior of human osteoblast cells and the coating improved the viability of the cells.

To determine whether cells could grow, attach, and interact with the 3D tubular scaffolds, SEM and fluorescence analysis were performed to observe the morphology of cultured hFOB cells. For fluorescence analysis, a representative SEM image of the surface of 3D tubular scaffolds with and without fiber coating is shown (Figures 12(a) and 12(e)). From the SEM and fluorescence analysis, the images show that osteoblasts cells adhered to and grew on the surface of the scaffold (Figures 10–12). The cells appeared to attach well on the 3D PLA tubular scaffold coated with fibers where osteoblasts cover all of the surface of the scaffold and on the reinforced spun fibrous morphology where the lamellipodia projection of their cytoplasm could be seen after interacting with neighboring cells that could contribute to the

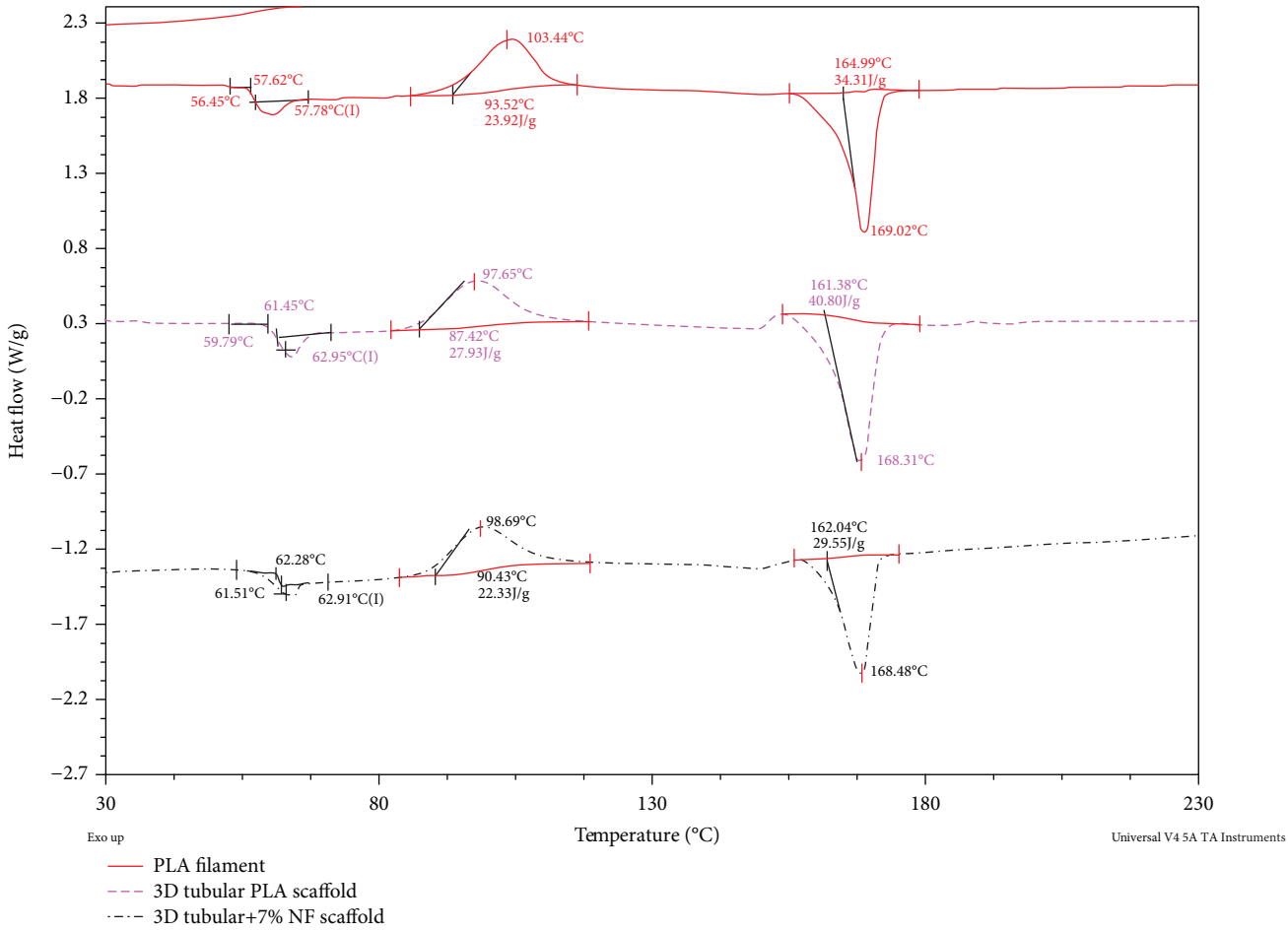

Figure 7: DSC thermograms of the PLA filament (red), 3D tubular scaffold (purple), and 3D tubular scaffold coated with nanofibers (black).

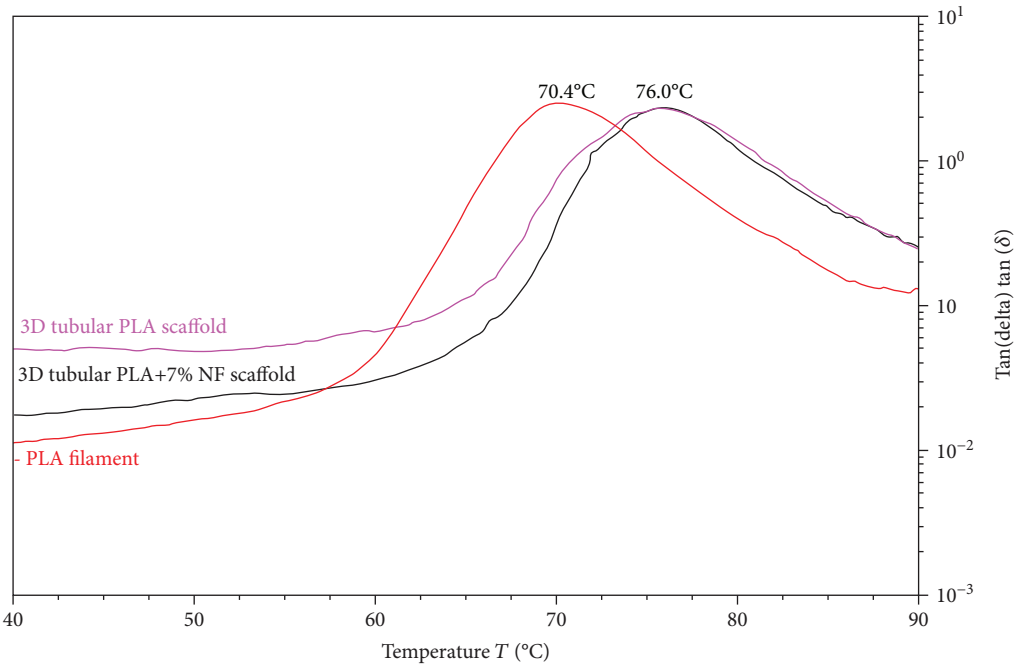

Figure 8: DMA results of the PLA filament (red), 3D tubular scaffold (purple), and 3D tubular scaffold coated with nanofibers (black).

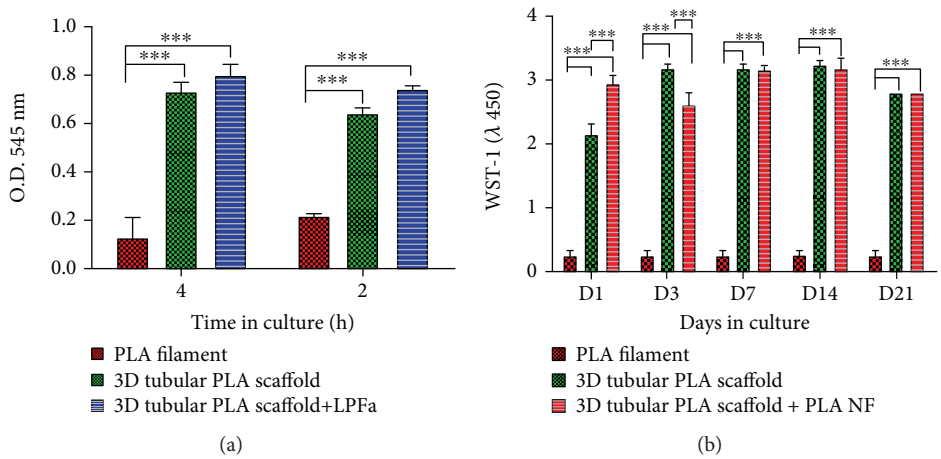

Figure 9: Biocompatibility response of human fetal osteoblasts seeded onto the 3D-printed tubular scaffold. (a) Cell adhesion at 4 and 24 h of cell culture. (b) WST assay showing the viability of cells evaluated at 1 to 21 days of cell culture. Statistical significance is indicated by $^{*}p < 0.05$.

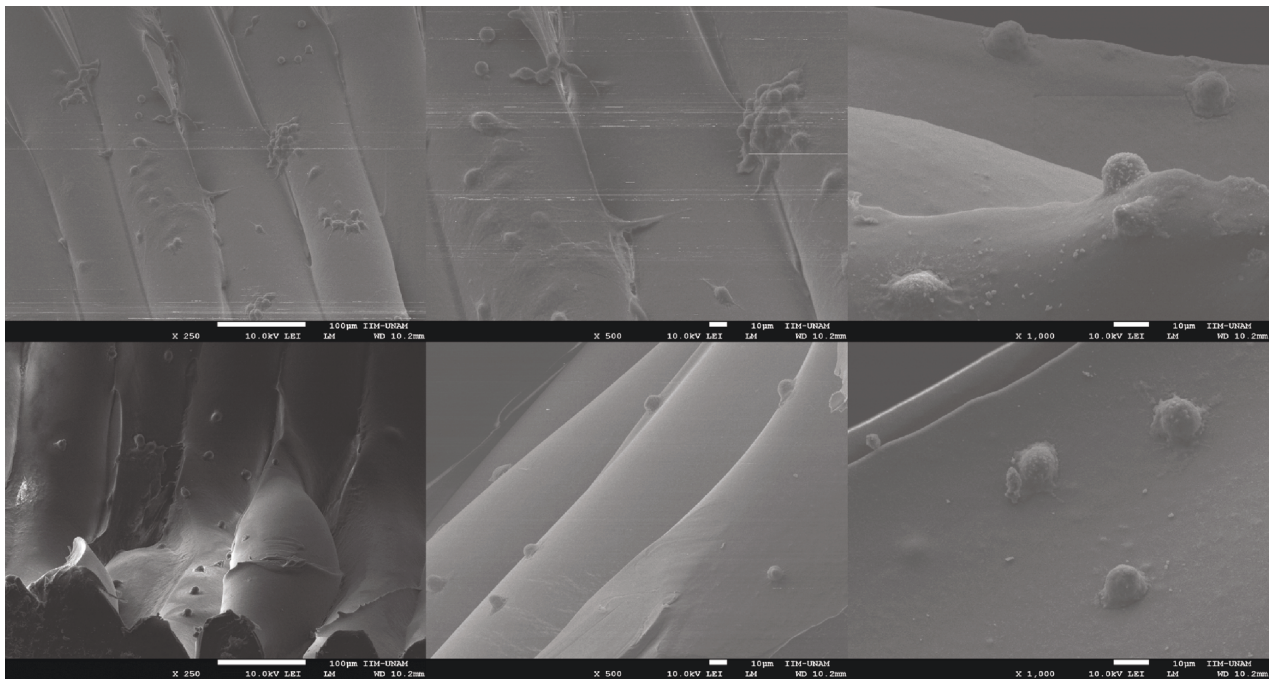

Figure 10: SEM micrographs of the 3D tubular scaffold surface seeded with hFOB cells showing some cells with an oval to spindle-shaped morphology typical of osteoblasts cells.

formation of deposited tissue as shown by SEM images (Figure 10). After the osteoblast cells attached to the surface of these scaffolds, a widened distribution with cellular extensions or lamellipodia was revealed to have contact with other cells and with the surface, maintaining a polygonal characteristic morphology as shown by the fluorescence images (Figures 12(f)–12(h)). Moreover, the hFOB cells on the 3D tubular scaffold also showed a cell affinity with isolated cells or with cells in small disperse groups over the surface, presenting a rounded cytoplasm with few spreading cells that exhibited a flat shape as shown by SEM (Figure 11) and fluorescence micrography (Figures 12(b)–12(d)). From the cell-material interaction analysis of the spreading and morphology of hFOB cells, the 3D tubular scaffold did not induce visible changes in cellular morphology and is not cytotoxic, indicating that the nanotopology surface is more favorable for the spread of osteoblast cells supporting the cell adhesion assay where cells adhered to a greater degree on the 3D tubular scaffold coated with fibers and indicating that the scaffolds were more favorable for cell adhesion and proliferation than the 3D PLA tubular scaffold without coating. This coating gives to the 3D tubular scaffold a property that is important in bone tissue engineering because the success of the scaffold for bone induction depends on the scaffold design for controlled geometries, i.e., a specific microenvironment by surface topography that

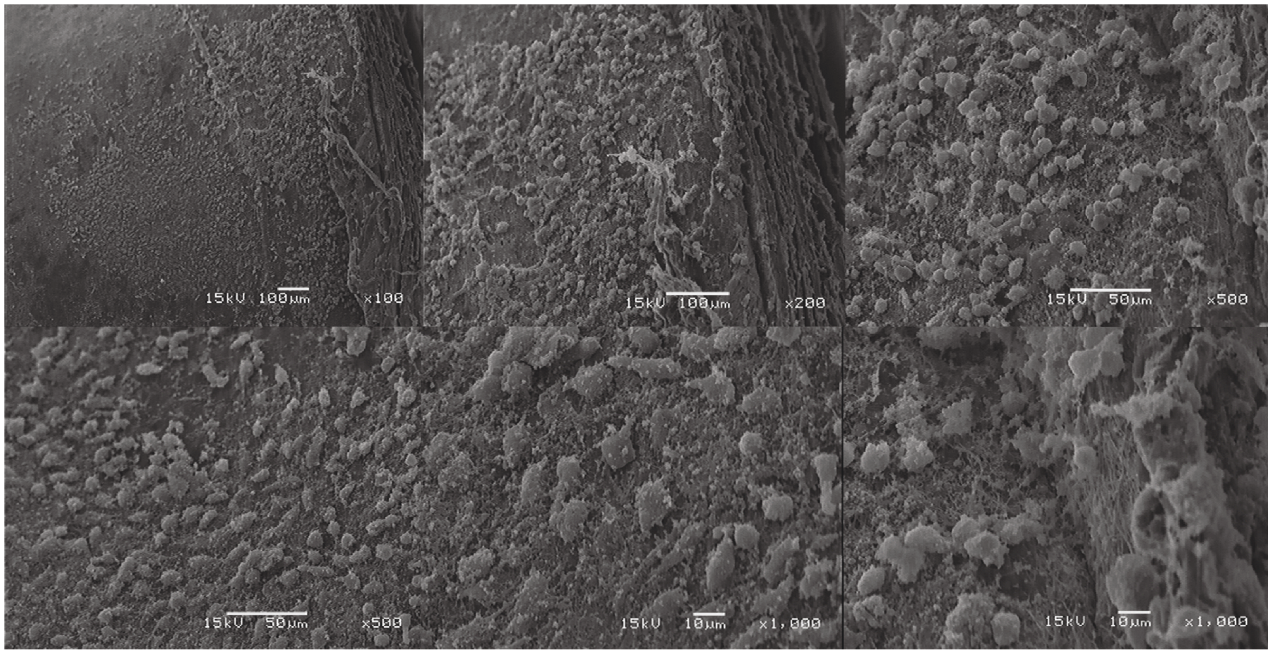

Figure 11: SEM micrographs of the 3D tubular scaffold coated with nanofibers showing the surface seeded with hFOB cells, where a good spread of the cells with a spindle-shaped morphology was observed typical of osteoblast cells with the projection of the cell-material interaction.

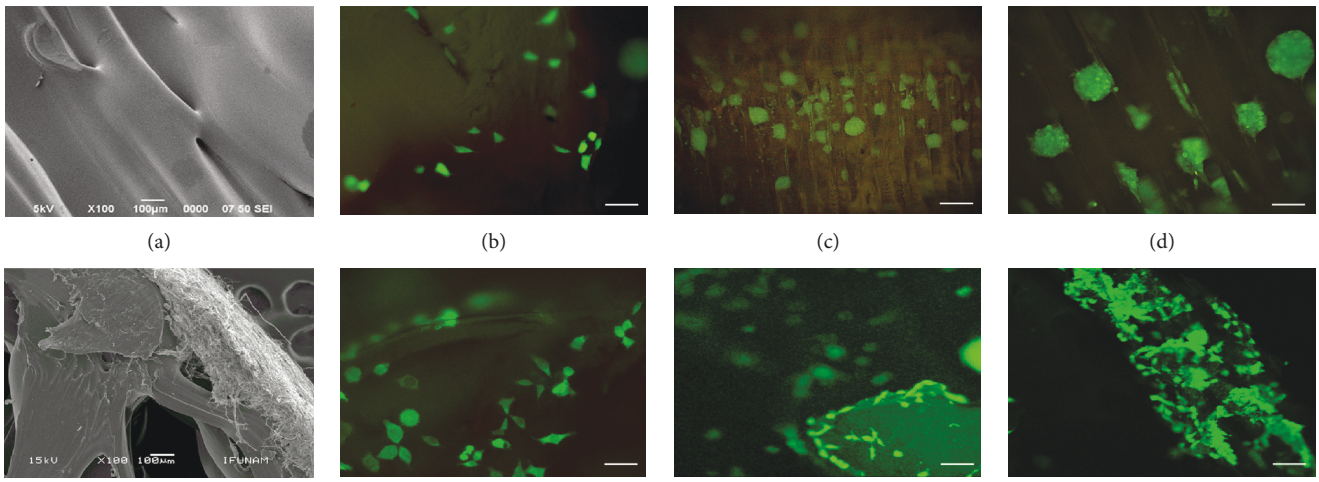

Figure 12: Fluorescence images of the cell-material interaction of hFOB cells seeded onto the 3D tubular scaffold (b–d) and onto the 3D tubular scaffold coated with nanofibers (f–h). Scale bar = 50 μm. A representative SEM micrograph is shown for the surface of the tubular scaffold (a, e).

improves cell biological response to the material allowing the promotion of osteoblast activity and bone deposit formation [44, 45]. The 3D tubular scaffold produced in this study allows expecting the detection of the differentiation of hFOB cells into mature osteoblasts because the coating of the fiber layer should mimic the structural and biochemical functions of the natural extracellular matrix of bone. This imitation is important for cell attachment and proliferation as we reported in the study; however, it could also stimulate the cell differentiation and mineralization of the osteoblasts. This expected differentiation response by surface characteristics could start with the induction of a common marker of osteoblasts (such as alkaline phosphatase) as an early marker of bone formation, and then the scaffolds may provide osteoconductive communication with the surrounding cells for the expression of noncollagenous proteins that regulated the 3D nodules and mineral deposit as a later marker of bone differentiation. Moreover, considering our preliminary results, we propose that the 3D tubular scaffold presented in this study is a promising material that could facilitate

mineralization for future guided bone regeneration applications. However, more studies on the differentiation properties of the 3D tubular scaffold need to be performed.

4. Conclusion

The additive manufacturing technique employing an ordinary commercial 3D printer has been successfully used for the fabrication of a 3D scaffold with a defined tubular shape and an inner structure that provided regular and sufficient porosity. Moreover, the successfully fabricated 3D tubular scaffold was homogeneously coated by a layer of submicrometric fiber membrane by the AJS technique. The 3D surface of the printed tubular scaffold exhibited distinctive morphologies and structures analyzed by SEM, and the surface roughness of the tubular scaffolds increased with the incorporation of the coating functionalization by the fiber membrane. Moreover, scaffolds coated with submicrometric fibers allow hFOB cells to adhere and proliferate better than uncoated 3D tubular scaffolds showing that the fibers work as a platform to improve cell biocompatibility (being not toxic to cells) and provide support to colonization and cell growth by the osteoblast cells. Moreover, the 3D tubular scaffold coated with fibers needs more studies as a biomineralization process in order for it to have a potential future use in bone tissue engineering or for it to have an application in the vascularization process.

Data Availability

All data generated or analyzed during this study are included in this manuscript.

Conflicts of Interest

The authors declare that they have no conflict of interest and no financial interest related to this study.

Acknowledgments

The authors want to thank Raul Reyes Ortíz and Adriana Tejeda Cruz from IIM-UNAM and M. en C. Jaqueline Cañetas from IFUNAM for their technical assistance and Dr. Esteban Avendaño from CICIMA-UCR, for his technical support in the profilometry analysis. FCVV and OACC wish to thank CONACYT for their doctoral scholarship (No. 297735 and No. 331089) during this study. This work was supported by the DGAPA-UNAM program PAPIIT IT203618 and the CONACYT A1-S-9178 projects.

References

[1] N. Chanchareonsook, R. Junker, L. Jongpaiboonkit, and J. A. Jansen, "Tissue-engineered mandibular bone reconstruction for continuity defects: a systematic approach to the literature," *Tissue Engineering. Part B, Reviews*, vol. 20, no. 2, pp. 147–162, 2014.

[2] J. E. Babensee, J. M. Anderson, L. V. McIntire, and A. G. Mikos, "Host response to tissue engineered devices," *Advanced Drug Delivery Reviews*, vol. 33, no. 1-2, pp. 111–139, 1998.

[3] W. R. Shelton, L. Papendick, and A. D. Dukes, "Autograft versus allograft anterior cruciate ligament reconstruction," *Arthroscopy*, vol. 13, no. 4, pp. 446–449, 1997.

[4] R. Tevlin, A. McArdle, D. Atashroo et al., "Biomaterials for craniofacial bone engineering," *Journal of Dental Research*, vol. 93, no. 12, pp. 1187–1195, 2014.

[5] A. Atala, F. K. Kasper, and A. G. Mikos, "Engineering complex tissues," *Science Translational Medicine*, vol. 4, no. 160, p. 160rv12, 2012.

[6] J. Henkel, M. A. Woodruff, D. R. Epari et al., "Bone regeneration based on tissue engineering conceptions—a 21st century perspective," *Bone Research*, vol. 1, no. 3, pp. 216–248, 2013.

[7] Y. Kinoshita and H. Maeda, "Recent developments of functional scaffolds for craniomaxillofacial bone tissue engineering applications," *The Scientific World Journal*, vol. 2013, Article ID 863157, 21 pages, 2013.

[8] R. Tevlin, G. G. Walmsley, O. Marecic, M. S. Hu, D. C. Wan, and M. T. Longaker, "Stem and progenitor cells: advancing bone tissue engineering," *Drug Delivery and Translational Research*, vol. 6, no. 2, pp. 159–173, 2016.

[9] S. Tajbakhsh and F. Hajiali, "A comprehensive study on the fabrication and properties of biocomposites of poly (lactic acid)/ceramics for bone tissue engineering," *Materials Science and Engineering C*, vol. 70, pp. 897–912, 2017.

[10] L. Roseti, V. Parisi, M. Petretta et al., "Scaffolds for bone tissue engineering: state of the art and new perspectives," *Materials Science and Engineering C*, vol. 78, pp. 1246–1262, 2017.

[11] B. S. Kim, S. S. Yang, and C. S. Kim, "Incorporation of BMP-2 nanoparticles on the surface of a 3D-printed hydroxyapatite scaffold using an ε-polycaprolactone polymer emulsion coating method for bone tissue engineering," *Colloids and Surfaces B: Biointerfaces*, vol. 170, pp. 421–429, 2018.

[12] S. Bose, S. Vahabzadeh, and A. Bandyopadhyay, "Bone tissue engineering using 3D printing," *Materials Today*, vol. 16, no. 12, pp. 496–504, 2013.

[13] R. Dorati, C. Colonna, C. Tomasi, I. Genta, G. Bruni, and B. Conti, "Design of 3D scaffolds for tissue engineering testing a tough polylactide-based graft copolymer," *Materials Science and Engineering C*, vol. 34, pp. 130–139, 2014.

[14] A. Grémare, V. Guduric, R. Bareille et al., "Characterization of printed PLA scaffolds for bone tissue engineering," *Journal of Biomedial Materials Research Part A*, vol. 106, no. 4, pp. 887–894, 2018.

[15] A. F. Balogová, R. Hudák, T. Tóth et al., "Determination of geometrical and viscoelastic properties of PLA/PHB samples made by additive manufacturing for urethral substitution," *Journal of Biotechnology*, vol. 284, pp. 123–130, 2018.

[16] M. Rabionet, E. Polonio, A. Guerra, J. Martin, T. Puig, and J. Ciurana, "Design of a scaffold parameter selection system with additive manufacturing for a biomedical cell culture," *Materials*, vol. 11, no. 8, p. 1427, 2018.

[17] A. Bruyas, F. Lou, A. M. Stahl et al., "Systematic characterization of 3D-printed PCL/β-TCP scaffolds for biomedical devices and bone tissue engineering: influence of composition and porosity," *Journal of Materials Research*, vol. 33, no. 14, pp. 1948–1959, 2018.

[18] K. K. Gómez-Lizárraga, C. Flores-Morales, M. L. del Prado-Audelo, M. A. Álvarez-Pérez, M. C. Piña-Barba, and C. Escobedo, "Polycaprolactone- and polycaprolactone/ceramic-based 3D-bioplotted porous scaffolds for bone regeneration: a comparative study," *Materials Science &*

Engineering. C, Materials for Biological Applications, vol. 79, pp. 326–335, 2017.

[19] G. Narayanan, V. N. Vernekar, E. L. Kuyinu, and C. T. Laurencin, "Poly (lactic acid)-based biomaterials for orthopaedic regenerative engineering," *Advanced Drug Delivery Reviews*, vol. 107, pp. 247–276, 2016.

[20] A. Denchai, D. Tartarini, and E. Mele, "Cellular response to surface morphology: electrospinning and computational modeling," *Frontiers in Bioengineering and Biotechnology*, vol. 6, p. 155, 2018.

[21] M. V. Granados-Hernández, J. Serrano-Bello, J. J. Montesinos et al., "*In vitro* and *in vivo* biological characterization of poly(lactic acid) fiber scaffolds synthesized by air jet spinning," *Journal of Biomedical Materials Research Part B, Applied Biomaterials*, vol. 106, no. 6, pp. 2435–2446, 2018.

[22] D. H. Rosenzweig, E. Carelli, T. Steffen, P. Jarzem, and L. Haglund, "3D-printed ABS and PLA scaffolds for cartilage and nucleus pulposus tissue regeneration," *International Journal of Molecular Sciences*, vol. 16, no. 12, pp. 15118–15135, 2015.

[23] A.-M. Haaparanta, E. Järvinen, I. F. Cengiz et al., "Preparation and characterization of collagen/PLA, chitosan/PLA, and collagen/chitosan/PLA hybrid scaffolds for cartilage tissue engineering," *Journal of Materials Science: Materials in Medicine*, vol. 25, no. 4, pp. 1129–1136, 2014.

[24] Y. Zhuang, W. Song, G. Ning et al., "3D-printing of materials with anisotropic heat distribution using conductive polylactic acid composites," *Materials & Design*, vol. 126, pp. 135–140, 2017.

[25] R. T. L. Ferreira, I. C. Amatte, T. A. Dutra, and D. Bürger, "Experimental characterization and micrography of 3D printed PLA and PLA reinforced with short carbon fibers," *Composites Part B: Engineering*, vol. 124, pp. 88–100, 2017.

[26] B. Wittbrodt and J. M. Pearce, "The effects of PLA color on material properties of 3-D printed components," *Additive Manufacturing*, vol. 8, pp. 110–116, 2015.

[27] Y. Tao, H. Wang, Z. Li, P. Li, and S. Q. Shi, "Development and application of wood flour-filled polylactic acid composite filament for 3d printing," *Materials*, vol. 10, no. 4, p. 339, 2017.

[28] B. A. Khan, H. Na, V. Chevali, P. Warner, J. Zhu, and H. Wang, "Glycidyl methacrylate-compatibilized poly(lactic acid)/hemp hurd biocomposites: processing, crystallization, and thermo-mechanical response," *Journal of Materials Science & Technology*, vol. 34, no. 2, pp. 387–397, 2018.

[29] H. Kaczmarek, M. Nowicki, I. Vuković-Kwiatkowska, and S. Nowakowska, "Crosslinked blends of poly(lactic acid) and polyacrylates: AFM, DSC and XRD studies," *Journal of Polymer Research*, vol. 20, no. 3, p. 91, 2013.

[30] R. Revati, M. S. Abdul Majid, M. J. M. Ridzuan et al., "Mechanical, thermal and morphological characterisation of 3D porous *Pennisetum purpureum*/PLA biocomposites scaffold," *Materials Science and Engineering: C*, vol. 75, pp. 752–759, 2017.

[31] G. Cicala, D. Giordano, C. Tosto, G. Filippone, A. Recca, and I. Blanco, "Polylactide (PLA) filaments a biobased solution for additive manufacturing: correlating rheology and thermomechanical properties with printing quality," *Materials*, vol. 11, no. 7, p. 1191, 2018.

[32] A. Gregor, E. Filová, M. Novák et al., "Designing of PLA scaffolds for bone tissue replacement fabricated by ordinary commercial 3D printer," *Journal of Biological Engineering*, vol. 11, no. 1, 2017.

[33] W. Xu, A. Pranovich, P. Uppstu et al., "Novel biorenewable composite of wood polysaccharide and polylactic acid for three dimensional printing," *Carbohydrate Polymers*, vol. 187, pp. 51–58, 2018.

[34] T. Serra, M. Ortiz-Hernandez, E. Engel, J. A. Planell, and M. Navarro, "Relevance of PEG in PLA-based blends for tissue engineering 3D-printed scaffolds," *Materials Science and Engineering: C*, vol. 38, pp. 55–62, 2014.

[35] T. Serra, J. A. Planell, and M. Navarro, "High-resolution PLA-based composite scaffolds via 3-D printing technology," *Acta Biomaterialia*, vol. 9, no. 3, pp. 5521–5530, 2013.

[36] M. Wang, P. Favi, X. Cheng et al., "Cold atmospheric plasma (CAP) surface nanomodified 3D printed polylactic acid (PLA) scaffolds for bone regeneration," *Acta Biomaterialia*, vol. 46, pp. 256–265, 2016.

[37] R. H. Sanatgar, C. Campagne, and V. Nierstrasz, "Investigation of the adhesion properties of direct 3D printing of polymers and nanocomposites on textiles: effect of FDM printing process parameters," *Applied Surface Science*, vol. 403, pp. 551–563, 2017.

[38] G. Cicala, G. Saccullo, I. Blanco et al., "Polylactide/lignin blends: effects of processing conditions on structure and thermo-mechanical properties," *Journal of Thermal Analysis and Calorimetry*, vol. 130, no. 1, pp. 515–524, 2017.

[39] X. Li, Y. Wang, Z. Wang et al., "Composite PLA/PEG/nHA/dexamethasone scaffold prepared by 3D printing for bone regeneration," *Macromolecular Bioscience*, vol. 18, no. 6, article 1800068, 2018.

[40] T. Patrício, M. Domingos, A. Gloria, U. D'Amora, J. F. Coelho, and P. J. Bártolo, "Fabrication and characterisation of PCL and PCL/PLA scaffolds for tissue engineering," *Rapid Prototyping Journal*, vol. 20, no. 2, pp. 145–156, 2014.

[41] H.-J. Chung, E.-J. Lee, and S.-T. Lim, "Comparison in glass transition and enthalpy relaxation between native and gelatinized rice starches," *Carbohydrate Polymers*, vol. 48, no. 3, pp. 287–298, 2002.

[42] O. Martin and L. Averous, "Poly (lactic acid): plasticization and properties of biodegradable multiphase systems," *Polymer*, vol. 42, no. 14, pp. 6209–6219, 2001.

[43] D. Drummer, S. Cifuentes-Cuéllar, and D. Rietzel, "Suitability of PLA/TCP for fused deposition modeling," *Rapid Prototyping Journal*, vol. 18, no. 6, pp. 500–507, 2012.

[44] J. Babilotte, V. Guduric, D. Le Nihouannen, A. Naveau, J. C. Fricain, and S. Catros, "3D printed polymer-mineral composite biomaterials for bone tissue engineering: fabrication and characterization," *Journal of Biomedical Materials Research Part B: Applied Biomaterials*, vol. 00B, pp. 1–17, 2019.

[45] S. Midha, M. Dalela, D. Sybil, P. Patra, and S. Mohanty, "Advances in 3D bioprinting of bone: progress and challenges," *Journal of Tissue Engineering and Regenerative Medicine*, pp. 1–21, 2019.